Photofield emission from transition-metal surface states

Y. Gao and R. Reifenberger

Department of Physics, Purdue University, West Lafayette, Indiana 47907

(Received 31 March 1986; revised manuscript received 17 November 1986)

Studies of photofield emission from surface states on W(100), Mo(100), and Ir(111) are reported. The yield of photofield electrons from the W(100) surface states are analyzed for photon energies between 2.41 and 3.54 eV. The polarization dependence of the photofield current from W(100) and Ir(111) surface states is measured and found to depend on the normal component of the vector potential **A**. Little evidence for the nonlocal coupling of the different components of **A** at a transition-metal surface is found.

I. INTRODUCTION

It is generally recognized that the nonlocal response of an electron gas to an electromagnetic wave produces significant deviations in the **E** and **H** fields derived from the standard Fresnel formulas. These deviations are especially important at a metal-vacuum interface where the electron gas is characterized by a strong density variation over a length scale of a few angstroms. The study of electrons photoemitted from surface states provides a unique capability to probe the nature of an electromagnetic wave near a metal surface. Experimental measurements of the photoemitted electrons from surface states are therefore useful because they further our understanding of a radiation field near a metal surface at a microscopic level.

Prior studies designed to investigate this problem have reported on photoemission from free-electron-like metals at photon energies $\hbar\omega$ comparable to the plasmon energy $\hbar\omega_p$.[1] Existing theoretical work has concentrated on model calculations of free-electron jellium metals terminated by a sharp interface.[2,3] Little work has been reported in the low-photon-energy regime ($\hbar\omega < 0.25\hbar\omega_p$). Furthermore, since most theories are devoted to simplified models, little is known about the modifications to the electromagnetic fields in the immediate vicinity of a transition-metal surface. Effects related to the d-electron density profile at the metal-vacuum interface as well as the dielectric response of these electrons can be expected.

In this paper we report measurements of electrons photoemitted from surface states by incident laser radiation covering the visible and near-ultraviolet regions of the electromagnetic spectrum. The experiments were performed using photofield emission, a developing technique which allows the study of electrons photoexcited by low-energy photons to final states not accessible in standard photoemission measurements.[4–10] In a photofield emission experiment, monochromatic light is focused onto a field emitter and the photoemission energy distribution is observed. The photon energy is less than the work function of the emitting surface ($\hbar\omega < \Phi$), so that a sufficiently strong electric field ($\approx 10^9$ V/m) must be applied to the surface to allow the photoexcited electrons to escape into the vacuum. By measuring the photofield emission from initial states, localized at the metal surface, one can be as-

ured that electromagnetic effects at the metal-vacuum interface are probed.

The intent of this paper is to investigate what information can be extracted about the behavior of an electromagnetic wave at a transition-metal surface by using photofield emission from surface states. Ideally, one would like to directly measure the variation of the radiation field at the metal-vacuum interface as a function of photon energy. Deviations from the standard Fresnel predictions are anticipated due to the nonlocal dielectric response of the system. A resulting modification to the photoyield and polarization dependence of the photoemission cross section might be expected. The measurements reported in this paper may broaden the limited contact between experiment and theory and ultimately lead to a more realistic treatment of transition-metal surfaces. Preliminary aspects of this study have already been reported elsewhere.[10]

The remainder of this paper is divided into the following sections. In Sec. II we briefly give some theoretical considerations. The apparatus used in the measurements are described in Sec. III. The data are presented and analyzed in Sec. IV. In Sec. V we summarize the important results of our study.

II. THEORETICAL CONSIDERATIONS

The photoexcitation of an electron from an initial state $|i\rangle$ to a final state $|f\rangle$ can be analyzed through the matrix element M_{fi}:

$$M_{fi} = \langle f | \mathbf{A}\cdot\mathbf{p} + \mathbf{p}\cdot\mathbf{A} | i \rangle , \tag{1}$$

where **A** is the vector potential of the incident radiation field and **p** is the momentum operator. It is generally known that the evaluation of Eq. (1) must include two contributions. One involves a treatment of the potential in which an electron is located. The second includes the spatial variation of the vector potential. A discussion of the matrix element relevant to this paper has been discussed elsewhere.[11] The approximation for **A** in Eq. (1) is of particular interest. In what follows, **A** is written as $A_0\hat{\epsilon}$, where $\hat{\epsilon}$ is the direction of the polarization vector. We assume a metal surface defined by an x-y plane and

choose the plane of incidence to be the y-z plane. Thus the angle of incidence of the electromagnetic radiation is defined with respect to the surface normal $\hat{n}$.

In Ref. 11 it was shown that Eq. (1) can be simplified under certain conditions. The essential simplifications concern approximation for the surface potential barrier and the behavior of **A** near the metal surface. If the potential barrier at a metal-vacuum interface can be approximated by a sharp step of height V_0 and when the derivative of **A** at the interface is given by

$$\frac{\partial A_0}{\partial z} = A_0(0_-)[\epsilon(\omega) - 1]\delta(z) , \tag{2}$$

where $\epsilon(\omega)$ is the metal dielectric constant and $A_0(0_-)$ is the vector potential evaluated just inside the $z = 0$ plane, then M_{fi} can be written as

$$M_{fi} = \frac{2i}{\hbar\omega}\hat{\epsilon}\cdot\hat{z}A_0(0_-)\Gamma , \tag{3}$$

where

$$\Gamma = V_0\left[\frac{2W}{V_0}\right]^{1/2}\left[1 - [\epsilon(\omega) - 1]\left[\frac{\hbar\omega}{2V_0} + \frac{2W}{V_0} + \frac{i[(W+\omega)(V_0 - W)]^{1/2}}{V_0}\right]\right] . \tag{4}$$

In Eq. (3), $\hbar\omega$ is the energy of the incident photons, and W is the energy of the initial state electrons and is defined in terms of their total energy E by $E = (\hbar k_{||})^2/2m + W$.

In the study of photoemission from a surface state, the photosignal is expected to be particularly sensitive to the approximation used for $A_0(z)$. Theories based on a free-electron jellium model show a coupling of the various components of **A** in the surface region. In general, an additional surface contribution to the z component of the vector potential can be anticipated. This modification to A_z^0 by the surface region is usually written as an integral equation of the form[12]

$$\overline{A}_z(z) \propto \frac{4\pi i}{\omega}\int_{z_1}^{z_2}[\sigma_{zx}(z,z')A_x^0(z')$$

$$+ \sigma_{zz}(z,z')A_z^0(z')]dz' , \tag{5}$$

where $\overline{A}_z$ is the surface modification to A_z^0, σ_{zx} and σ_{zz} are the conductivity components which can be related to the elementary excitation spectrum of the metal, and the limits on the integral specify the spatial extent of the "surface region." Although it seems generally accepted that this coupling will occur, most theories avoid a numerical comparison of σ_{zx} and σ_{zz}. Furthermore, since A_x^0 is continuous across the interface, it can become larger than A_z^0 which suffers a strong attenuation at the metal surface. Thus, even though σ_{zx} may be less than σ_{zz}, the net contribution of the σ_{zx} term in Eq. (5) may be comparable to the σ_{zz} contribution. It would be interesting to determine the relative importance of the σ_{zx} component to $\overline{A}_z$ and further analysis of the experimental results presented below may ultimately provide this information for low photon energies.

The experiments described below are sensitive to two quantities, the $\hbar\omega$ variation of M_{fi} and the polarization dependence of M_{fi}. The nonlocality will evidently change the value of $A_0(0_-)$ appearing in Eq. (3). In addition, any nonlocal effects will significantly alter the evaluation of terms related to the spatial variation of **A** because various components of the incident electromagnetic wave can couple together in a complicated way. If the coupling between the components of **A** is significant, the polarization

dependence of the Eq. (3) could become complicated. Otherwise this term will have the simple $\hat{\epsilon}\cdot\hat{z}$ polarization signature given in Eq. (3).

III. EXPERIMENTAL APPARATUS

Most of the experimental apparatus used to measure the photofield emission energy distribution in this study have been described previously.[8,13,14] The incident laser beam is focused with a high-resolution mirror mount onto a tungsten field emitter through a quartz converging lens of focal length 350 mm. The field emitter is enclosed in a UHV chamber ($P \leq 6 \times 10^{-11}$ Torr) to prevent gas contamination of the surface. By adjusting a precision manipulator, the field-emission tip can be accurately aligned to the probe hole of an electron energy analyzer situated below the emitter. The signal from a channeltron electron multiplier is accumulated by an online computer which also provides means of adjusting several experimental parameters.

The energy analyzer is composed of a retardation analyzer and a 127° differential analyzer in tandem. The 127° analyzer has been enclosed in a high-permeability μ-metal shield to screen stray magnetic fields. The resolution of the analyzer has been estimated to be better than 70 meV.[14]

An argon-ion laser operating in the single-line mode is used to illuminate the field emitter. The polarization of the beam can be rotated by a two-rhomb half-wave retarder mounted before the focusing lens. The laser was always operated in the output locking mode when the data were taken. Typical power flux density is about 10^8 W/m² on the field emitter.

The samples were prepared by electrochemical etching in a 1N sodium hydroxide (NaOH) solution.[15,16] Typical clean field-emission patterns were observed which helped to identify the orientations of the field emitters to be along [110] for W and Mo,[15] and [111] for Ir.[17]

The field emitter can be cleaned in situ by passing a sufficient dc current through the supporting loop of the emitter. Since the surface states are sensitive to surface

contamination, it becomes important to clean the field emitter in a reproducible fashion. In these experiments, this was attempted by using a timed flashing circuit that delivered a fixed current to the supporting loop for a preset period of time. In this way, the adsorbed gasses from the tip could be removed in a reproducible fashion. In addition, all data obtained were from a well annealed field emitter that had reached its equilibrium end shape. Thus, even though the field emitter is momentarily raised to a high temperature between different data runs, the overall shape of the emitter did not change appreciably. Typical time for taking one photofield energy distribution was about 10 min, a time short enough to ensure that the surface contamination was below 0.05 monolayer by the end of a data run.

IV. RESULTS AND DISCUSSIONS

It is useful to summarize the general features of the surface states that were chosen for study. W(100) is one of the most studied metallic surfaces.[18] One reason is that W(100) supports a surface state with energy ~ 0.35 eV below the Fermi energy E_F. The surface state was first observed by Swanson and Crouser as an anomalous emission feature in a field-emission energy distribution (FEED) study.[19] Subsequent observations using field emission[20] and photoemission[21] identified the surface nature of this state. Theoretical calculations have been reported that estimate about 90% of the surface state is localized within the first atomic layer of the W(100) surface.[22]

Molybdenum resides in the same column of the Periodic Table as tungsten and the two elements have many properties in common. Mo(100) supports a surface state which was also observed in field emission. Photoemission and field-emission studies have shown that the Mo(100) surface state has similar properties as W(100) except that it lies ≈ 0.2 eV below E_F.[23–25]

In contrast to tungsten and molybdenum, the Ir(111) surface state is known to have considerably different characteristics. The first observation of a structure ≈ 0.40 eV below E_F was reported by Dionne and Rhodin in a field-emission study.[26] They attributed the structure to effects of the bulk electronic bands.[27] Later study revealed that the structure can be suppressed by absorption of gas molecules and the structure was then identified as due to a surface state.[28] In contrast to the W(100) or Mo(100) surface state, the surface state on Ir(111) is not readily observed in photoemission.[29] Surprisingly, it takes several monolayers of CO to suppress the surface-emission structure in field emission,[28] much more than the fraction of a monolayer needed to totally suppress the W(100) and Mo(100) surface states.[20] This puzzle was partly answered by a combined study of field evaporation and field emission performed by Yiet et al.[30] By selective termination of field evaporation, a flat Ir(111) surface or a stepped surface could be produced. It was found that the surface-state structure in field emission occurred only on the stepped surface and it was concluded that the surface state on Ir(111) was associated with the presence of surface terraces.

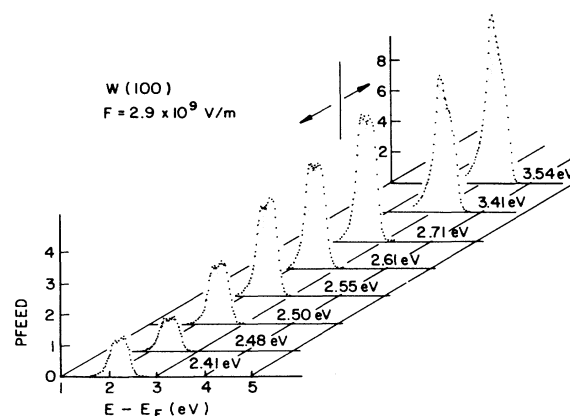The photofield emission technique is suitable for

FIG. 1. Photofield-emission energy distribution from W(100) for photon energies from 2.41 to 3.54 eV. The surface feature, located at $\hbar\omega - 0.35$ eV, is shown by the shaded region in each of the distributions. For uv lines (3.41 eV, 3.54 eV), the surface-state feature dominates the photofield-emission energy distribution.

measuring photoemission from transition metal surface states over a range of photon energies readily obtained from commercial lasers. This is illustrated in Fig. 1 which shows the measured photofield energy distributions from W(100) for 2.4 eV $< \hbar\omega <$ 3.6 eV.

The expected shape of the photofield energy distribution (PFEED) was derived by Schwartz and Cole.[31,32] In their theory the total energy distribution is given by

$$\frac{dj(E)_{\mathrm{pf}}}{dE} = -\frac{e^3}{2\hbar^4\omega^3}\frac{n}{\Omega}(\hat{e}\cdot\hat{z})^2 f(E - \hbar\omega)$$

$$\times \int_{-V_0+\hbar\omega}^{E} dW \frac{D(W)|\Gamma|^2}{\sqrt{W(W - \hbar\omega)}}, \qquad (6)$$

where n/Ω is the photon density, $f(E)$ is the Fermi-Dirac distribution, and $D(W)$ is the transmission probability for an electron to traverse the surface potential barrier with energy $E = W + (\hbar k_{\parallel})^2/2m$. In writing Eq. (6), the zero of E is taken to be the vacuum level. The quantity Γ is proportional to the relevant matrix elements as defined in Eqs. (3) and (4) above.

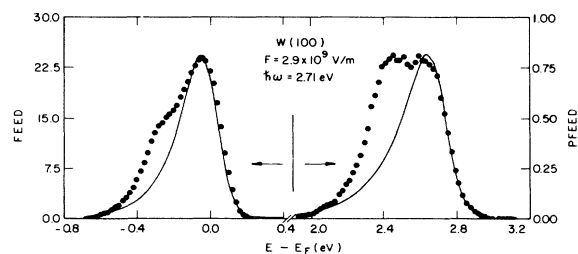The expression for $dj(E)_{\mathrm{pf}}/dE$ given by Eq. (6) can be

FIG. 2. Photofield-emission energy distribution from W(100) for $\hbar\omega = 2.71$ eV. The distribution near E_F is from field-emitted electrons (FEED). The distribution near $E_F + \hbar\omega$ is from photofield-emitted electrons (PFEED). The solid curves are theoretical expectations without the surface state. The surface feature at -0.35 eV in FEED is enhanced in PFEED.
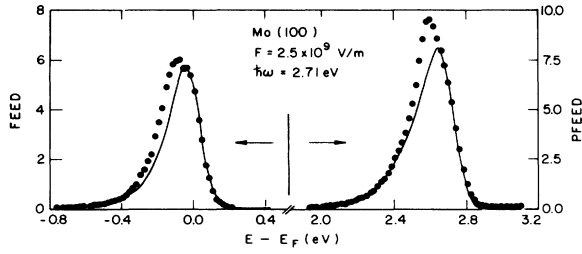
FIG. 3. Photofield-emission energy distribution from Mo(100) for $\hbar\omega = 2.71$ eV. The distribution near E_F is from field-emitted electrons (FEED). The distribution near $E_F + \hbar\omega$ is from photofield-emitted electrons (PFEED). The solid curves are theoretical expectations without the surface state. The surface feature at -0.20 eV in FEED is enhanced in PFEED.

FIG. 4. Photofield-emission energy distribution from Ir(111) for $\hbar\omega = 3.54$ eV. The distribution near E_F is from field-emitted electrons (FEED). The distribution near $E_F + \hbar\omega$ is from photofield-emitted electrons (PFEED). The solid curves are theoretical expectations without the surface state. The surface feature at -0.40 eV in FEED is enhanced in PFEED.

evaluated and fit to the experimental data in Fig. 1. When this is done, it is easy to determine the excess number of electrons emitted from the surface state. This surface-state emission feature is shown by the shaded regions in each of the photoexcited energy distributions in Fig. 1.

Figures 2—4 show details of the surface-state features from W(100), Mo(100), and Ir(111) in both field emission and photofield emission at selected photon energies. The shape of the photofield distribution based on Eq. (6) is shown by the solid lines in these figures. The shape of the energy distribution of field-emitted electrons is also plotted in Figs. 2—4 and is based on a standard result that has been derived in many places:[33]

$$\frac{dj(E)_{\text{fe}}}{dE} = \frac{J_0}{d} \frac{e^{(E-E_F)/d}}{1+e^{(E-E_F)/k_BT}} . \tag{7}$$

In Eq. (7), J_0 is a constant and d is a parameter that depends on the work function and electric field strength applied to the metal surface. The other parameters used in Eqs. (6) and (7) were obtained in the usual ways.[8,11,13] The Fermi energy E_F is estimated from the field-emission data by fitting to a calculated field-emission energy distribution using Eq. (7). The electric field F is obtained from the well-known Fowler-Nordheim plot.[33] The transmission probability through the image rounded surface potential barrier was determined numerically.[34] The conduction-band depth V_0 (Refs. 32, 35, and 36) and the work function Φ of the facets[37-39] were taken from the literature and are listed in Table I. The temperature rise of the field emitter under laser illumination was also taken into account as described elsewhere.[40]

A general characteristic of the data shown in these figures is the considerable enhancement of the surface-state feature in photofield emission when compared to the
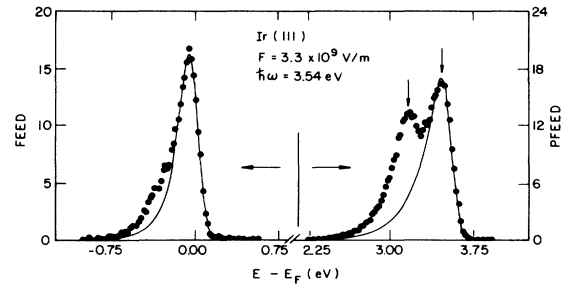
field-emission distributions. In order to determine the photocurrent emitted from the surface states, as a function of $\hbar\omega$, the magnitude of the photofield emission calculation [Eq. (6)] is scaled to fit the measured energy distribution. This procedure is adopted since the area from which the emitted electrons are detected cannot be accurately determined. By subtracting the theoretical fits from the data, it is possible to estimate the current emitted from the surface state.

In fitting the model calculations to the experimental energy distributions, several practical difficulties were encountered. For instance, it was found that the results from Mo(100) were difficult to interpret because the surface-state contribution coincides with the peak in the photofield data. This causes some uncertainty in scaling the theoretical calculations to experimental data. A further complication arises because the low melting point of Mo requires a lower flashing temperature which in turn causes uncertainties in producing a surface free from adsorbed gasses. Difficulties of a different nature were encountered in analyzing data from Ir(111). Because of the high work function of Ir, it was difficult to obtain statistically good data at the lower photon energies. As a result, the study on Ir(111) was confined to the blue and ultraviolet lines from the laser. In what follows, we concentrate on the yield from the W(100) surface state as a function of photon energy and the polarization dependence of the surface-state emission from W(100) and Ir(111).

A. Yield from W(100) surface state as a function of photon energy

To measure the yield of the surface state as a function of photon energy, the size of the surface-state signal must be estimated from the data shown in Fig. 1. This was

TABLE I. A list of the parameters used in photofield-emission energy distribution calculations.

	Conduction-band depth from vacuum level (eV)		Work function (eV)	
W(100)	-10.8	(Ref. 32)	4.93	(Ref. 37)
Mo(100)	-11.4	(Ref. 35)	4.45	(Ref. 38)
Ir(111)	-16.4	(Ref. 36)	5.76	(Ref. 39)

done by subtracting the fit based on Eq. (6) from the experimental data and integrating the signal originating from the surface state. In order to normalize out small variations due to differences in the tip condition, we find it useful to form the ratio of this surface-state signal to the area under the field-emission energy distribution that was taken at the same time. In this way we normalize out the unknown emission area of our tip, remove the effect of small variations in the work function which inevitably occur in this type of study, and minimize the uncertainty in the determination of the strength of the applied electric field.

The relative yield defined in this way is plotted in Fig. 5 for two different data runs. The data taken at low photon energies are quite reproducible, but some scatter is clearly evident in the uv range. The photon energy dependence of the relative yield can also be estimated from Eq. (6). In this calculation, a number of simplifying approximations were necessary. The terms in Eq. (4) depending on the spatial variation of $\mathbf{A}$ were neglected. The surface-state wave function was assumed to be free-electron-like in order to estimate $\langle f(0) | i(0) \rangle$. The integration of the surface-state emission feature was restricted to a 40-meV region centered about this peak. This region of the surface-state photocurrent is most accurately determined by our data analysis procedure outlined above.

To take the reflectivity of the surface into account, the

vector potential near the surface was estimated using the expression[41]

$$\frac{A_z(z)}{A_0} = - \frac{\sin(2\theta_i)}{\frac{z}{\alpha}[\epsilon(\omega)-1]+\frac{1}{2}[\epsilon(\omega)+1]}$$

$$\times \frac{\epsilon(\omega)}{[\epsilon(\omega)-\sin^2\theta_i]^{1/2}+\epsilon(\omega)\cos\theta_i} , \quad (8)$$

where θ_i is the incident angle, α describes the region in which $\epsilon(\omega)$ changes linearly from 1 to the bulk value. The magnitude of α is a few angstroms. The incident photon energy n/Ω was estimated from the measured laser power and beam width[6] and the yields are normalized to a free-space photon density $(n/\Omega)_n = 10^9/4.8\pi$ cm^{-3} as described previously.[11] The values of $\epsilon(\omega)$ for W were taken from Ref. 42. In calculating the theoretical curve, shown in Fig. 5, $z = 0.25\alpha$ was assumed as suggested in Ref. 41. The present calculation does little more than predict the upward trend in the photofield yield as $\hbar\omega$ increases. Including terms related to the spatial variation of $\mathbf{A}$ will certainly increase the the calculated photoyield, a feature that is required from Fig. 5. If more information about the surface-state wave function and density of states were known, this calculation could be extended to provide a more quantitative and realistic comparison of theory to experiment.

B. Polarization dependence of photofield emission from W(100)

Since the surface-state contribution to the photofield energy distribution is known to be localized within the first atomic layer of the metal surface, it is of interest to examine the polarization dependence of the surface-state photocurrent. This aspect of our data has already been discussed elsewhere[10] and is included here for the sake of completeness.

The surface-state contribution to the photofield emission signal as a function of polarization orientation is shown in Fig. 6. The geometry of the incident beam is shown as the inset of Fig. 6. The angle between the polarization vector $\hat{e}$ and surface normal $\hat{z}$ is defined as Ψ. The solid curve in Fig. 6 is the calculated polarization dependence assuming an $\hat{e} \cdot \hat{z}$ behavior found in Eq. (3). The reasonable agreement between the simple model and the $\cos^2\Psi$ variation suggests that longitudinal components of $\mathbf{A}$ are not strongly produced near the metal surface by nonlocal effects. It also indicates that the parallel periodicity of the surface potential is not important in determining the polarization dependence of the photofield current from the W(100) surface state.

C. Polarization dependence of photofield emission from Ir(111)

As discussed above, the Ir(111) surface state is different in origin from the W(100) surface state, and it is therefore interesting to see if there is any difference in the polarization dependence. It is also worth noticing that since the Ir(111) surface state is associated with surface terraces, it
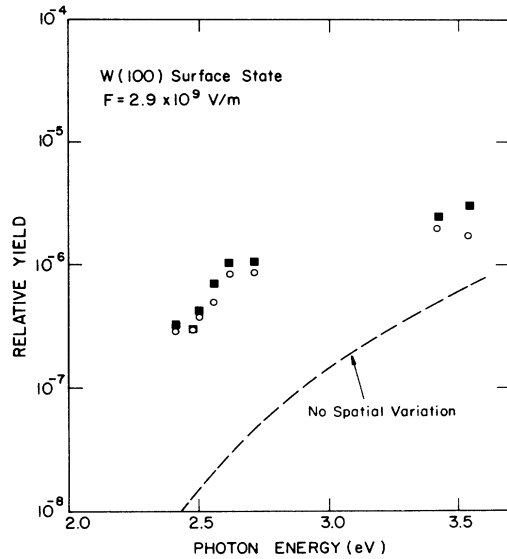
FIG. 5. Photofield-electron yield from W(100) surface state for photon energies from 2.41 to 3.54 eV. The solid squares are from data shown in Fig. 1 and the open circles are from another data run. They are obtained from the experimental results by subtracting the theory curve from the observed spectrum and integrating the remaining surface state contribution. The theoretical yield neglecting the spatial variation of $\mathbf{A}$ is also plotted on the figure. Since the surface-state density of states is not known, the comparison of the theory to the experiment is at best only qualitative.
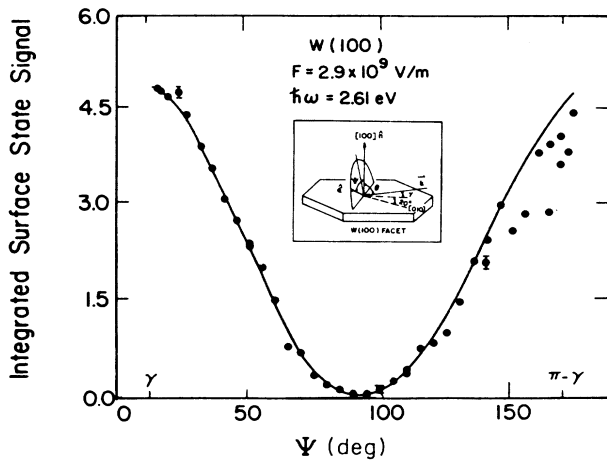
FIG. 6. The polarization dependence of the photofield-emission current from the W(100) surface state. The inset shows the relevant geometrical considerations. The solid curve is $\cos^2\Psi$ where Ψ is the angle between the surface normal $\hat{n}$ and the polarization direction $\hat{e}$ of the incident light.
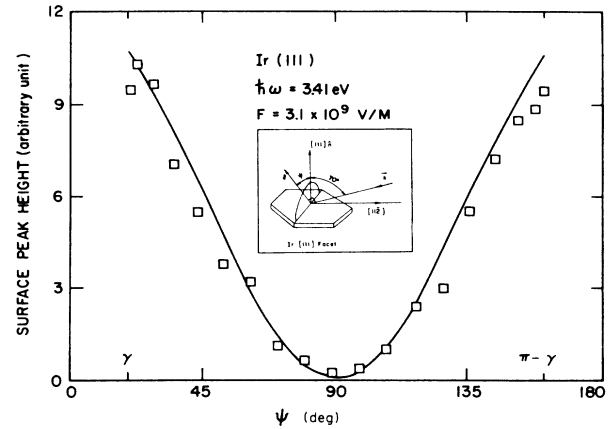

FIG. 7. The polarization dependence of the peak height of the Ir(111) (100) surface state. The solid curve is $\cos^2\Psi$ where Ψ is the angle between the surface normal $\hat{n}$ and the polarization direction $\hat{e}$ of the incident light. The inset shows the relevant geometrical considerations.

makes an ideal system to check if the parallel component of the surface potential is important.

The polarization dependence is obtained in a way slightly different from that in tungsten. Only two energies in the photofield emission energy distributions, marked with arrows in Fig. 4, have been monitored. The higher energy ($E_1 \equiv E - E_F \approx 3.5$ eV) is not influenced by the surface state while the other energy ($E_2 \equiv E - E_F \approx 3.2$ eV) is chosen to coincide with the peak in the surface-state contribution. By monitoring the signal at two final-state energies, it is possible to scan all polarization directions in a short period of time, thereby avoiding difficulties due to frequent flashing of the field emitter during data acquisition. The surface-state contribution is deduced by subtracting the measured signal at energy E_2 from the calculated PFEED contribution evaluated at the same energy. It is also assumed that for any polarization of the incident laser beam, the calculated PFEED can be scaled to the measured PFEED by a multiplicative factor determined by the peak height of the measured PFEED at energy E_1. For the case of Ir(111), where the surface-state signal is well separated from the peak in the photofield energy distribution, this procedure is quite reasonable.

The surface-state signal from Ir(111) as a function of the polarization angle Ψ is shown in Fig. 7. The geometry of the incident light is illustrated in the inset of Fig. 7. The analyzed data exhibit good agreement to $\cos^2\Psi$ which is drawn as a solid curve in the same figure. The reasonable agreement between the data and the $\cos^2\Psi$ variation indicates that the longitudinal components in A are not strongly produced near the metal surface by the nonlocal effects. Furthermore, the parallel periodicity of the surface potential is not important even in terraced Ir(111).

The size of the photofield signal from the surface state for s polarized light ($\Psi = 90°$ in Fig. 7) is reduced by a factor of ≈ 25 from its value at $\Psi = 20°$. This should be contrasted to a reduction by a factor of ≈ 70 for photo-

field emission from the W(100) surface state (Fig. 6) taken under similar geometrical conditions. From the considerations leading to Eq. (3), the emission from a surface state should be completely suppressed for s-polarized light. The fact that surface emission from Ir(111) is considerably larger than the emission from the W(100) surface state may be an indication of the different characteristics of these two surface states.

In general, the reasonable agreement between the data and the $\cos^2\Psi$ variation indicates that the longitudinal components in A are not strongly produced near the metal surface by the nonlocal effects. Furthermore, the parallel periodicity of the surface potential is not important even on terraced Ir(111).

V. CONCLUSIONS

In this paper we present the results of an experimental study of photofield emission from surface states on W(100), Mo(100), and Ir(111). The photofield yield from the W(100) surface state is measured for photon energies 2.41 eV $< \hbar\omega <$ 3.54 eV and analyzed in the context of a simple model that includes the standard Fresnel variation of the vector potential at the metal surface. The polarization dependence of the photofield current from W(100) and Ir(111) surface states are also presented. The data show that the polarization dependence of the surface state depends on the normal component of the vector potential A. This behavior indicates that the coupling between the component of A introduced by the surface is not strong. Another conclusion which can be drawn from the polarization study is that the surface potential can be reliably described as a variation along the surface normal only, even for the surface state on Ir(111) which is known to be associated with surface terraces.

ACKNOWLEDGMENTS

[1]H. J. Levinson and E. W. Plummer, Phys. Rev. B **24**, 628 (1981).

[2]K. L. Kliewer, Phys. Rev. B **14**, 1412 (1976).

[3]P. J. Feibelman, Phys. Rev. B **14**, 762 (1976).

[4]M. J. G. Lee, Phys. Rev. Lett. **30**, 1193 (1973).

[5]T. Radon and Ch. Kleint, Surf. Sci. **60**, 540 (1976).

[6]R. Reifenberger, H. A. Goldberg, and M. J. G. Lee, Surf. Sci. **83**, 599 (1979).

[7]R. Reifenberger, C. M. Egert, and D. L. Haavig, J. Vac. Sci. Technol. A **2**, 927 (1984).

[8]D. L. Haavig and R. Reifenberger, Surf. Sci. **151**, 128 (1985).

[9]D. Venus and M. J. G. Lee, Surf. Sci. **125**, 452 (1983).

[10]Y. Gao and R. Reifenberger, Phys. Rev. B **32**, 1380 (1985).

[11]Y. Gao and R. Reifenberger, Phys. Rev. B (to be published).

[12]G. Mukhopadhyay and S. Lundqvist, Phys. Scr. **17**, 69 (1978).

[13]C. M. Egert and R. Reifenberger, Surf. Sci. **145**, 159 (1984).

[14]Y. Gao and R. Reifenberger, J. Phys. E **18**, 381 (1985).

[15]R. H. Good and E. W. Muller, in *Handbuch der Physik*, edited by S. Flugger (Springer-Verlag, Berlin, 1956), Vol. 21.

[16]N. J. Dionne and T. N. Rhodin, Phys. Rev. B **14**, 322 (1976).

[17]J. M. Derochette and J. Marien, Phys. Status Solidi A **39**, 281 (1977).

[18]B. Feuerbacher and R. F. Willis, J. Phys. C **9**, 169 (1976).

[19]L. W. Swanson and L. C. Crouser, Phys. Rev. Lett. **16**, 389 (1966).

[20]E. W. Plummer and J. W. Gadzuk, Phys. Rev. Lett. **25**, 1493 (1970).

[21]Shang-Lin Weng, T. Gustasson, and E. W. Plummer, Phys. Rev. Lett. **39**, 822 (1977).

[22]M. Posternak, H. Krakauer, A. J. Freeman, and D. D. Koelling, Phys. Rev. B **21**, 5601 (1980).

[23]Shang-Lin Weng, Phys. Rev. Lett. **38**, 434 (1977).

[24]R. V. Kasowski, Solid State Commun. **17**, 179 (1975).

[25]Shang-Lin Weng and E. W. Plummer, Solid State Commun. **23**, 515 (1977).

[26]N. J. Dionne and T. N. Rhodin, Phys. Rev. Lett. **32**, 1311 (1974).

[27]N. J. Dionne and T. N. Rhodin, Phys. Rev. B **14**, 322 (1976).

[28]K. Klapper, H. F. Kempin, and G. Ertl, Z. Phys. Chem. Neue Folge **112**, S45 (1978).

[29]P. A. Zhdan, G. K. Boreskov, A. I. Boronin, A. P. Schepelin, W. F. Egelhoff, Jr., and W. H. Weinberg, Surf. Sci. **71**, 267 (1978).

[30]D. Dao Yiet, N. Rihon, and J. C. P. Mignolet, Phys. Status Solidi A **58**, 501 (1980).

[31]C. Schwartz and M. W. Cole, Surf. Sci. **115**, 290 (1982).

[32]C. Schwartz, Ph.D. thesis (Pennsylvania State University, 1980).

[33]R. H. Fowler and L. W. Nordheim, Proc. R. Soc. London, Ser. A **199**, 173 (1928).

[34]R. Reifenberger, D. L. Haavig, and C. M. Egert, Surf. Sci. **109**, 276 (1981).

[35]D. D. Koelling, F. M. Mueller, A. J. Arko, and J. B. Ketterson, Phys. Rev. B **10**, 4889 (1974).

[36]G. O. Arbman and S. Hornfeldt, J. Phys. F **2**, 1062 (1972).

[37]S. Hellwig and J. H. Block, Z. Phys. Chem. **83**, 269 (1973).

[38]G. Bergeret, M. Abon, B. Tardy, and S. J. Teichner, J. Vac. Sci. Technol. **11**, 1193 (1974).

[39]R. W. Strayer, W. Mackie, and L. W. Swanson, Surf. Sci. **34**, 225 (1973).

[40]Y. Gao and R. Reifenberger, J. Vac. Sci. Technol. A **4**, 1289 (1986).

[41]A. Bagchi, N. Kar, and R. G. Barrera, Phys. Rev. Lett. **40**, 803 (1978).

[42]J. H. Weaver, C. Krafka, D. W. Lynch, and E. E. Koch, in *Optical Properties of Metals*, Vol. 18-1 of *Physik Daten*, (Fachinformationszentrum, Karlsruhe, 1981).